Chemistry Europe
European Chemical Societies Publishing

WILEY VCH

Excellence in Chemistry Research

Announcing our new flagship journal

- Gold Open Access
- Publishing charges waived
- Preprints welcome
- Edited by active scientists

Meet the Editors of *ChemistryEurope*

Luisa De Cola
Università degli Studi di Milano Statale, Italy

Ive Hermans
University of Wisconsin-Madison, USA

Ken Tanaka
Tokyo Institute of Technology, Japan

ChemCatChem

Research Article
doi.org/10.1002/cctc.202200665

Chemistry Europe
European Chemical Societies Publishing

www.chemcatchem.org

Particle Size Effects of Carbon Supported Nickel Nanoparticles for High Pressure CO_2 Methanation

Nienke L. Visser,[a] Oscar Daoura,[a] Philipp N. Plessow,[b] Luc C. J. Smulders,[a] Jan Willem de Rijk,[a] Joseph A. Stewart,[c] Bart D. Vandegehuchte,[c] Felix Studt,[b, d] Jessi E. S. van der Hoeven,[a] and Petra E. de Jongh*[a]

Supported nickel nanoparticles are promising catalysts for the methanation of CO_2. The role of nickel particle size on activity and selectivity in this reaction is a matter of debate. We present a study of metal particle size effects on catalytic stability, activity and selectivity, using nickel on graphitic carbon catalysts. Increasing the Ni particle size from 4 to 8 nm led to a higher catalytic activity, both per gram of nickel and normalized surface area. However, the apparent activation energy remained the same (~105 kJ mol^{-1}). Comparing experiments at atmospheric to 30 bar pressure demonstrates the importance of testing under industrially relevant pressures; the highest selectivity is obtained at high CO_2 conversions and pressures. Finally, the selectivity was particle size-dependent. The largest particles were not only most active but also most selective to methane. With this work we contribute to the ongoing debate about Ni particle size effects in CO_2 methanation.

Introduction

CO_2 hydrogenation to methane using green hydrogen is a valuable reaction to store renewable energy and produce synthetic natural gas.[1–3] CO_2 methanation, better known as the Sabatier reaction[4] proceeds according to the Equation 1:

$$CO_2 + 4H_2 \leftrightarrows CH_4 + 2H_2O$$
$$\Delta H^0 = -165\ \text{kJ mol}^{-1},\ \Delta S^0 = -172.5\ \text{J mol}^{-1}\ \text{K}^{-1}\ [5] \quad (1)$$

CO_2 methanation is thermodynamically favoured at low temperatures (150–300 °C at 1 bar) and elevated pressures (> 10 bar).[6] When increasing the pressure, the thermodynamically feasible temperature range enlarges. For example, at 400 °C, 96% conversion can be reached at 30 bar compared to 85% at 1 bar (calculated with HSC Chemistry,[7] taking into account H_2:CO_2 in a 4:1 ratio and CH_4, CO and H_2O as products). In the seventies and eighties of the last century, industrial processes in this field have consisted of the formation of syngas (CO and H_2) from coal, followed by the production of synthetic natural gas via methanation, for which typical reaction conditions were 25–80 bar and 300–500 °C.[8–10] Several (pilot) plants were commissioned for the hydrogenation of CO_2,[11] of which some are designed to operate at elevated pressures, even up to 30 bar.[12] With a technology readiness level (TRL) of 7,[13] there is still the need to further develop the technology. Despite the relevance to understand CO_2 methanation at high pressures, the vast majority of experimental papers reports catalytic testing at ambient pressure.

Supported nickel catalysts are well-known for their high activity and relatively low costs for this process. Factors that can influence the activity and selectivity of these catalysts, apart from reaction conditions, are for example the metal particle size[14,15] and type of support.[3,16–18] For metal particle sizes in the range between 2 and 20 nm, the ratio between more coordinated (terrace) and less coordinated (stepped) metal surface sites is relevant to the catalytic performance.[19] As a result, the intrinsic catalytic activity (per metal surface site) is an average value and may depend on the particle size.[19,20]

The concurrence of different reaction pathways can complicate a Ni particle size study on CO_2 methanation. The most commonly reported pathways occur either via the (hydrogen-assisted) formation of CO (the reversed water gas shift (RWGS) reaction), followed by direct or hydrogen-assisted CO dissociation, or via the formation of formate as intermediate.[16,21–24] Although it is generally accepted that CO methanation over Ni catalysts is structure sensitive and hence particle size-dependent,[25–27] there is no consensus yet about the occurrence

[a] N. L. Visser, Dr. O. Daoura, L. C. J. Smulders, J. W. de Rijk, Dr. J. E. S. van der Hoeven, Prof. P. E. de Jongh
Materials Chemistry and Catalysis
Debye Institute for Nanomaterials Science
Utrecht University
Universiteitsweg 99
3584 CG Utrecht (The Netherlands)
E-mail: P.E.deJongh@uu.nl
[b] Dr. P. N. Plessow, Prof. F. Studt
Institute of Catalysis Research and Technology
Karlsruhe Institute of Technology
76344 Eggenstein-Leopoldshafen (Germany)
[c] Dr. J. A. Stewart, Dr. B. D. Vandegehuchte
TotalEnergies OneTech Belgium
Zone Industrielle Feluy C
B-7181 Seneffe (Belgium)
[d] Prof. F. Studt
Institute for Chemical Technology and Polymer Chemistry
Karlsruhe Institute of Technology
76131 Karlsruhe (Germany)

Supporting information for this article is available on the WWW under https://doi.org/10.1002/cctc.202200665

This publication is part of a joint Special Collection with EurJOC and EurJIC on the Netherlands Institute for Catalysis Research. Please see our homepage for more articles in the collection.

of size effects in CO_2 methanation.[14,28] The role of Ni particle size and thus the concentration of surface corner, step and terrace sites in CO_2 methanation has been studied by both DFT and experiments. Lower coordinated sites were found to play an important role in activating CO_2 and CO, the intermediate product.[15,26,29–32] Concerning the activity of Ni catalysts in CO_2 methanation, different effects have been reported. There is still a debate whether there is an optimum in particle size (2–3 nm for Ni/SiO_2),[14] no particle size effect at all (>5 nm for Ni/AlO_2[28] and 3–9 nm for Ni/CNTs[33]) or an increase in activity with increasing size from 3 to 46 nm for Ni/CeO_2,[34] all reported in terms of turnover frequency (TOF). For Ni/MgO a significant increase in activity was observed when agglomerates were formed from single Ni sites during CO_2 methanation at 350 °C and 30 bar.[35]

For several metals an increase in particle size (up to ~9 nm) can direct the selectivity to CH_4.[15,17,36–38] Nickel nanoparticles have a higher selectivity to CH_4 than clusters,[15] possibly due to a decreased hydrogen coverage of smaller particles.[15,34,37] In the ultimate limit, single atoms could lack the ability to catalyse the multielectron reaction.[35] The formation of CO as side product must be carefully considered,[39] not only in terms of it being an undesired product, but also because its presence can negatively influence the CO_2 methanation activity.[40,41]

Carbon is used as support to prevent the strong interaction between nickel and oxidic supports[17,42] and thus the formation of for example nickel silicate[43] or nickel aluminate[44] species. These are difficult to reduce and might affect the study of particle size effects. Furthermore, carbon offers a high heat conductivity, especially with the use of graphitic carbon structures[33] and its low z-value allows for easy electron microscopy characterization, an important technique to analyse both the size and dispersion of nanoparticles.

In this study we investigated particle size and pressure effects for nickel on carbon catalysts for CO_2 methanation. To this end, a series of Ni/OxC catalysts with particle sizes varying from 3.7 to 7.6 nm was prepared and tested for CO_2 methanation at high (30 bar) and atmospheric pressure. We discuss the influence of particle size and pressure on both the activity and selectivity.

Results and Discussion

Preparation of catalysts with various Ni particle sizes

Nickel nanoparticles were deposited onto a carbon support with a graphitic sheetlike structure (graphene nanoplatelets, GNP-500) via incipient wetness impregnation. The carbon support was functionalized with oxidic surface groups (OxC) to create anchoring sites for the metal nanoparticles and enhance the stability of the catalysts. The particle size was varied via the Ni weight loading and heat treatment procedure. Figure 1A shows representative transmission electron microscopy (TEM) images of the nickel nanoparticles on functionalized carbon (Ni/OxC) with a surface averaged particle diameter (d_s) of

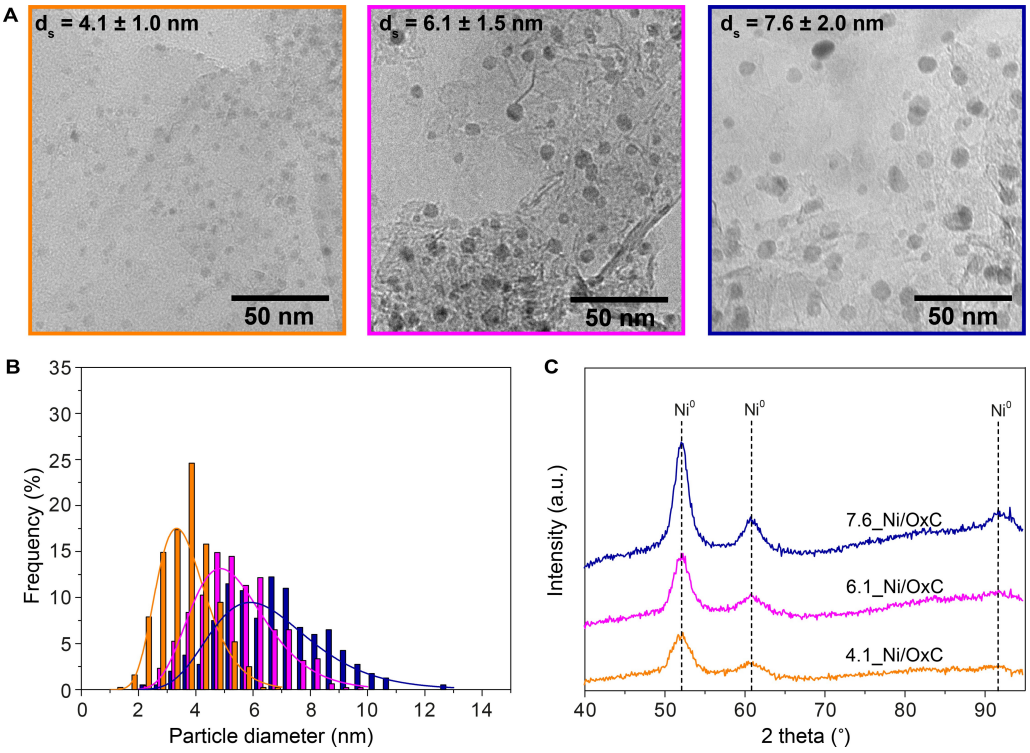

Figure 1. Nickel on carbon catalysts with different particle sizes. **A**) Representative TEM images of Ni/OxC catalysts with surface averaged nickel particle diameters of 4.1 ± 1.0 nm (orange, left), 6.1 ± 1.5 nm (magenta, middle) and 7.6 ± 2.0 nm (blue, right). **B**) Corresponding size distributions. **C**) X-ray diffractograms of the same Ni/OxC catalysts after subtraction of the OxC baseline.

4.1 ± 1.0 nm (orange, left), 6.1 ± 1.5 nm (magenta, middle) and 7.6 ± 2.0 nm (blue, right). Figure 1B demonstrates the corresponding size distributions, and Figure 1C the X-ray diffraction (XRD) patterns after subtraction of the carbon baseline. Altogether, different batches of Ni on carbon catalysts were prepared with an average TEM particle diameter varying from 3.7 to 7.6 nm (details of the full series can be found in Table 1, Table S1 and Figure S1, S2). Neither TEM nor XRD show evidence for large (>20 nm) Ni particles or crystallites in the samples. The experimental H_2 uptake determined by H_2 chemisorption was well in line with the TEM results for the catalysts with larger particles, however lower than expected with decreasing particle size (Figure S3, Table S2). Possible reasons for this deviation are more encapsulation or a lower degree of reduction of the smallest nanoparticles. Finally, the Ni weight loadings determined with thermographic analysis coupled with mass spectrometry (TGA-MS) (Table 1) closely matched the theoretical Ni loadings (Table S1).

After the catalyst synthesis, the metallic Ni/OxC catalysts were exposed to air. As a result, the Ni nanoparticles were passivated, e.g. the outer layer of the metal particles was oxidized. The re-reduction of these catalysts to obtain the metallic state of nickel, needed for CO_2 methanation, was followed with temperature programmed reduction (TPR). Figure 2 shows the presence of several peaks in the range of 150–340 °C, which are attributed to NiO reduction. H_2 consumption at temperatures above 380 °C (Figure S4) originated from support gasification, as was confirmed by MS measurements (Figure S5). This means that it is possible to reduce the NiO particles to metallic Ni at temperatures at which the carbon support remains mostly intact. The sample with the largest NiO particles exhibited the lowest reduction temperature (the main peak was located 202 °C for 7.6 nm Ni particles, sample 7.6_Ni/OxC, with only a small shoulder at 245 °C). For the 4.1 nm particles, the main NiO reduction peak shifted to 265 °C. The catalyst with intermediate sized nanoparticles (6.1 nm particles) showed two reduction peaks at intermediate temperatures, between 210 and 250 °C. The shift in reduction peak demonstrates that the reducibility of Ni depends on particle size.[27,45,46] For Ni/Al_2O_3, where the trend was opposite than shown in this study,[27] however, the effect of calcination temperature might have changed the interaction between the nickel and the support. Our trend matches results that were reported for silica-supported nickel, where an increase in reduction temperature indicates that nickel species interact more strongly with the support or even form nickel silicate species. As a result, full reduction is obtained only at temperatures up to 500–700 °C. [45,46] These kind of species that interact strongly with the support are not formed on carbon, making carbon supported nickel easier to reduce than silica supported nickel.[47]

Table 1. The Ni weight (wt) loading and particle diameter of fresh Ni/OxC catalysts.

Catalyst	Ni wt-loading[a] [wt%]	$d_s \pm \sigma_s$[b] [nm]	Ni^0 crystallite size[c] [nm]
3.7_Ni/OxC	4.5	3.7 ± 0.7	3.0
4.1_Ni/OxC	8.5	4.1 ± 1.0	3.8
4.6_Ni/OxC	8.3	4.6 ± 1.0	4.3
5.1_Ni/OxC	9.4	5.1 ± 1.0	4.3
6.1_Ni/OxC	9.3	6.1 ± 1.3	4.3
7.6_Ni/OxC	12.8	7.6 ± 1.9	5.0

[a] weight loading determined via TGA-MS [b] surface averaged particle diameters (d_s) and corresponding standard deviations (σ_s) determined with TEM. [c] Full-width at half-maximum XRD analysis of the Ni^0 peak at 52° after normalizing the diffractograms at the carbon (002) diffraction peak and subsequent subtraction of the OxC diffractogram.

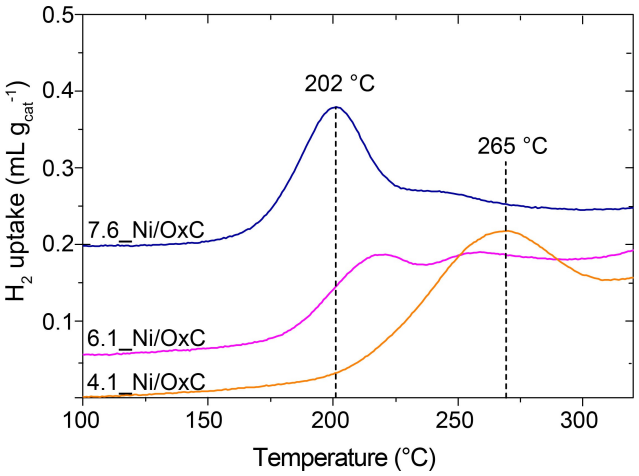

Figure 2. Reduction profiles of NiO_x nanoparticles with different sizes on the carbon support. The profiles are measured after passivation of the fresh Ni^0/OxC catalysts with an average nickel particle diameters of 4.1 ± 1.0 nm (orange), 6.1 ± 1.5 nm (magenta) and 7.6 ± 2.0 nm (blue) in air.

H_2-TPD showed lower adsorption temperatures for catalysts with larger particles in the temperature range of 300–450 °C (Figure S6). This can be explained by a weaker adsorption of H_2 on terrace sites than on step sites,[46] and/or a difference in H spillover to the support with changing Ni particle sizes.[48] To investigate the oxidation state of nickel in these catalysts and the interaction between Ni and the support, X-ray photoelectron spectroscopy (XPS) could be an interesting technique to use.[45] However, nickel is easily oxidized when exposed to air and it is difficult to use this technique under conditions mimicking reaction conditions.

Stability of nickel on oxidized carbon catalysts

In order to study the effect of Ni particle size, first the stability of the catalysts was examined. Figure 3A shows the CO_2 conversion of Ni/OxC catalysts at 300 °C and 30 bar as function of time on stream. After a slight activity loss during the first 20 h of reaction (15–17%), the Ni/OxC catalysts maintained a stable conversion over a time span of 100 h, regardless of the Ni particle size. At the same time, the data in Figure 3A indicate a correlation between catalytic activity and particle size. The largest particles (7.6 ± 2.0 nm) exhibited a higher conversion per gram of Ni. Also the highest CH_4 selectivity was obtained with the largest Ni particles. With decreasing particle size, a higher amount of CO was formed as side product (Figure 3B).

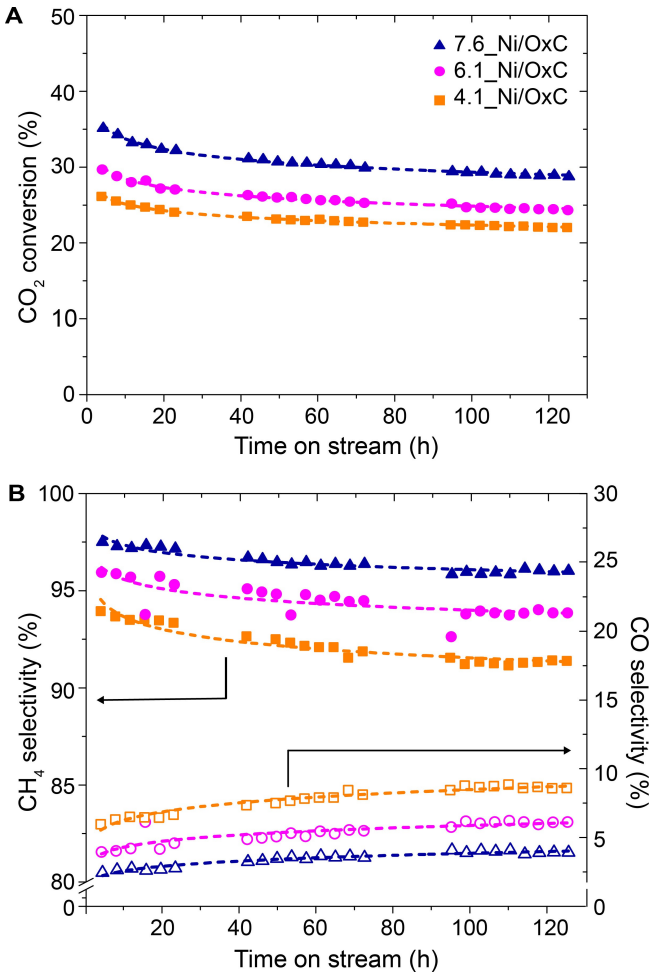

Figure 3. A) CO_2 conversion and **B**) CH_4 (closed symbols, left axis) and CO (open symbols, right axis) selectivity of Ni/OxC catalysts over 120 h on stream at 300 °C for catalysts with average nickel particle diameters of 4.1 ± 1.0 nm (orange), 6.1 ± 1.5 nm (magenta) and 7.6 ± 2.0 nm (blue). 4.6 mg Ni was loaded in each reactor. Reaction conditions: 30 bar, GHSV = 3500–5000 mL g_{cat}^{-1} h^{-1}.

To correlate the stability of the catalysts to their structural properties, the used catalysts were characterized with TEM and XRD. Electron microscopy analysis of the catalysts after CO_2 methanation showed that Ni particle growth was limited, but seemed more pronounced for the smaller particles (Table 2, Figure S7). The initial activity loss was independent of particle size. No significant carbon gasification occurred during catalysis and the sheet-like and graphitic nature of the catalysts was preserved (Figure S7, Table S4). Only on rare occasions, nickel nanoparticles that had grown significantly ($d > 50$ nm) were observed in the TEM analysis. These likely originated from local hot spots in the catalyst bed, despite the dilution with SiC, due to the exothermal nature of CO_2 methanation. X-ray diffraction analysis showed only the presence of small Ni^0 crystallites after catalysis for all catalysts (Figure S8). This confirmed that the fraction of the larger particles observed with TEM was minor. Most importantly, the stability of these Ni/OxC catalysts is sufficient to reliably measure the particle size effects at elevated temperatures and pressures.

Table 2. Ni particle diameters before (fresh) and after catalysis and the relative activity loss. Reaction conditions: 300 °C, 30 bar, GHSV = 3500–5000 mL g_{cat}^{-1} h^{-1}.

Catalyst	$d_s \pm \sigma_s$[a] fresh [nm]	$d_s \pm \sigma_s$[a] after catalysis [nm]	Activity loss after 120 h CO_2 methanation [%]
4.1_Ni/OxC	4.1 ± 1.0	5.9 ± 1.8	15.8
6.1_Ni/OxC	6.1 ± 1.3	6.5 ± 1.5	17.6
7.6_Ni/OxC	7.6 ± 1.9	7.7 ± 1.8	17.7

[a] surface averaged particle diameters (d_s) and corresponding standard deviations (σ_s) determined with TEM.

Influence of nickel particle size on the catalytic activity

The catalyst energetics were studied by varying the reaction temperature. Figure 4A displays the CO_2 conversion of the Ni/OxC catalysts at different temperatures. To minimize the effect of catalyst deactivation on the measurements, the catalysts were first stabilized at the highest temperature (340 °C) followed by a stepwise decrease in reaction temperature. After the initial stabilization period, steady state conversion could be assessed. The catalyst with the largest particles gave the highest conversion per gram Ni over the full temperature range, whereas the catalyst with the smallest Ni particles was the least active. This is in line with the trend observed in Figure 3A, which is nonetheless surprising, as smaller particles have a larger specific metal surface area. It was confirmed that the difference in conversion was not caused by variations in Ni weight loading. This was done by comparing two catalysts with different Ni loadings but similar particle diameters (3.4 wt% Ni, 3.5 ± 0.7 nm vs 10.1 wt% Ni, 3.9 ± 0.8 nm). The CO_2 conversion achieved could be correlated with particle size rather than nickel loading (Figure S9).

The data at 300 °C and 30 bar was used to calculate the specific activity of each catalyst. Figure 4B shows a 2 to 3-fold increase in turnover frequency (TOF) at 300 °C and 30 bar when increasing the Ni particle diameter from 4.8 to 7.7 nm, which confirmed the particle size dependence of the intrinsic catalytic activity. Using the Ni dispersion from H_2 chemisorption, the increase in activity with increasing particle size was confirmed (Figure S10). With chemisorption, it was only possible to determine the H_2 uptake of the fresh catalysts due to the amount of catalyst needed for the chemisorption measurements. For the calculation of the TOF based on TEM, particle diameters after catalysis were used, assuming that no further rearrangement of the catalysts had occurred after the initial stabilization period at the highest temperature. The smallest particles (4.1 nm) lostpercentagewise slightly less activity than the larger ones (7.6 nm), even though they grew relatively more during the initial hours of the catalytic test (Table 2). The fact that also the catalyst with Ni particles of 7.6 nm, which hardly displayed growth, lostactivity, suggests that other factors, such as restructuring of the nanoparticles might play a role. This seems to have a larger effect than the activity gain with particle

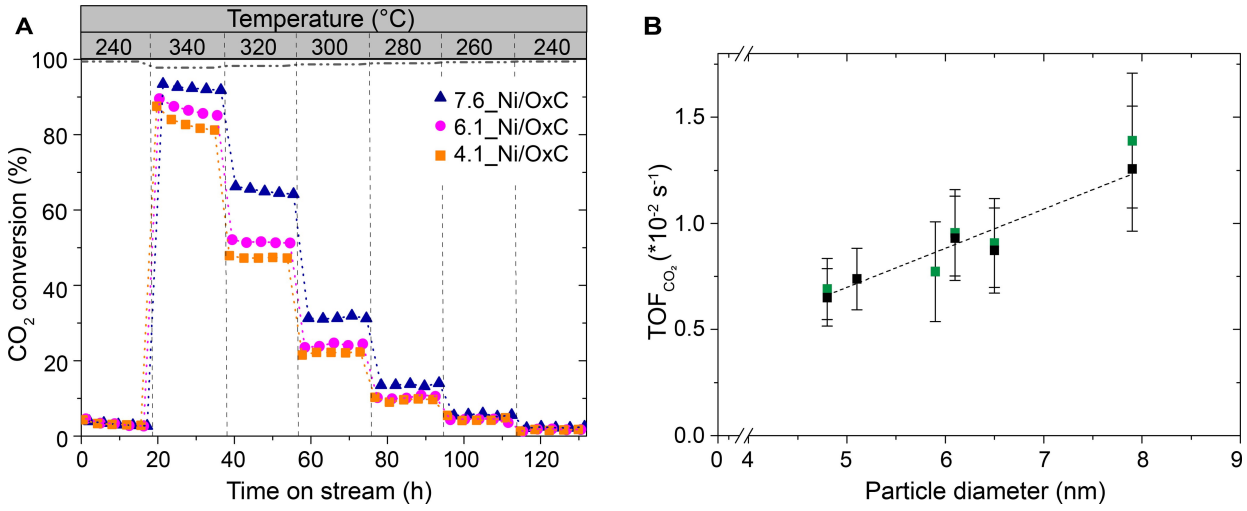

Figure 4. Particle size dependent activity at 30 bar. **A**) CO_2 conversion versus time on stream for the catalysts with d 4.1 (orange), 6.1 (magenta) and 7.6 nm (blue). 4.2 mg of nickel was loaded in each reactor. The grey dash-dotted line shows the equilibrium conversion. Reaction conditions: 240–340 °C, GHSV = 3500–5000 mL g_{cat}^{-1} h^{-1}. **B**) CO_2 turnover frequency (TOF) at 300 °C and 30 bar measured during two catalytic tests. Details of the tests are described in supporting information section I as *activity* (green) and *influence of pressure* (black). A linear fit is used as guide to the eye.

growth, expected with the higher nickel-based conversion and TOF for larger particles. To verify the reproducibility of the observed particle size effect, a second series of Ni/OxC catalysts with a Ni particle diameters of 3.5–9 nm was prepared (Table S5). For this series of catalysts the same trend of increasing TOF with Ni particle size was observed (Figure S11). TGA analysis (Figure S12, S13) shows that most of the surface groups have already decomposed during the synthesis or decompose during catalysis, from which we conclude that it is unlikely that variations in surface groups had a significant influence on the catalyst activity.

Despite the practical advantages to perform CO_2 methanation at high pressures, the vast majority of academic papers reports catalytic testing at ambient pressure, which might add complexity to the debate about particle size effects. Therefore, our Ni/OxC catalysts were also tested at atmospheric pressure (Figure 5). To allow a valid comparison of the activity of the catalysts at different pressures, we only compare data at the same conversion level (~20%), effectuated by adapting the inlet flow rate during the reaction (Figure S14). Relatively low conversions were targeted to allow studying the intrinsic catalyst properties and stay away from equilibrium conversions. Overall, lower pressures led to lower catalyst activities, which can be explained by the negative change in entropy for CO_2 methanation ($\Delta S^0 = -172.5$ J mol^{-1} K^{-1}),[5] and the fact that higher pressures shift the equilibrium to CH_4 formation. Most importantly, the trend of increasing TOF with increasing particle size was observed both at low and high pressures, albeit less pronounced at 1 bar.

To better understand the influence of Ni particle size on the activity, Arrhenius plots (Figure S15) were constructed from the data between 240 and 300 °C of Figure 4 to calculate the apparent activation energy (E_a), and apparent pre-exponential factor (Figure 6). The apparent activation energy was similar for

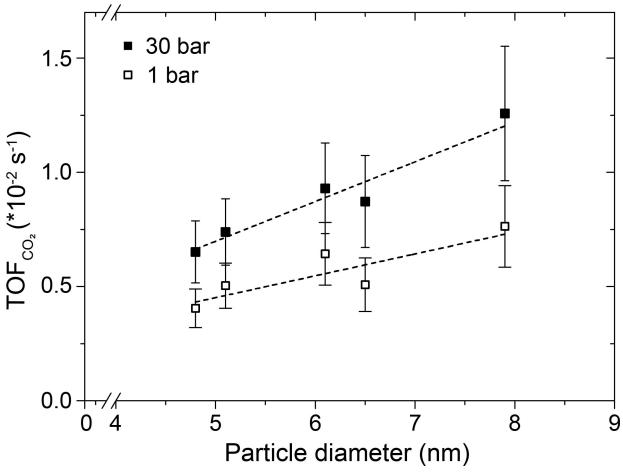

Figure 5. CO_2 turnover frequency (TOF) at 300 °C and 1 bar and 30 bar. The amount of catalyst loaded in the reactor and the flow were adjusted such that all catalysts were tested at approximately the same CO_2 conversions (~20%). The GHSV was varied between 1400–5000 mL g_{cat}^{-1} h^{-1} (1 bar) and 2500–9000 mL g_{cat}^{-1} h^{-1} (30 bar). The dashed lines are used as guide for the eye.

all particle sizes (103-107 kJ mol^{-1}) (Figure 6A). Rather, the increase in TOF can be correlated to the apparent pre-exponential factor (Figure 6B) and hence is likely due to a change in the fraction of active sites. From calculations for FCC particles in general[49] and a cube-octahedron Ni particle shape,[46] it is known that the amount of corner, step and terrace sites changes with particle size, where the abundance of corner and step sites decreases and the number of terrace sites increases with increasing particle sizes up to 10 nm. Between 4 and 8 nm, the amount of terrace sites approximately doubles,[46] which is quite well in line with our trend observed for activity (TOF). Hence, our observed increase in activity with increasing

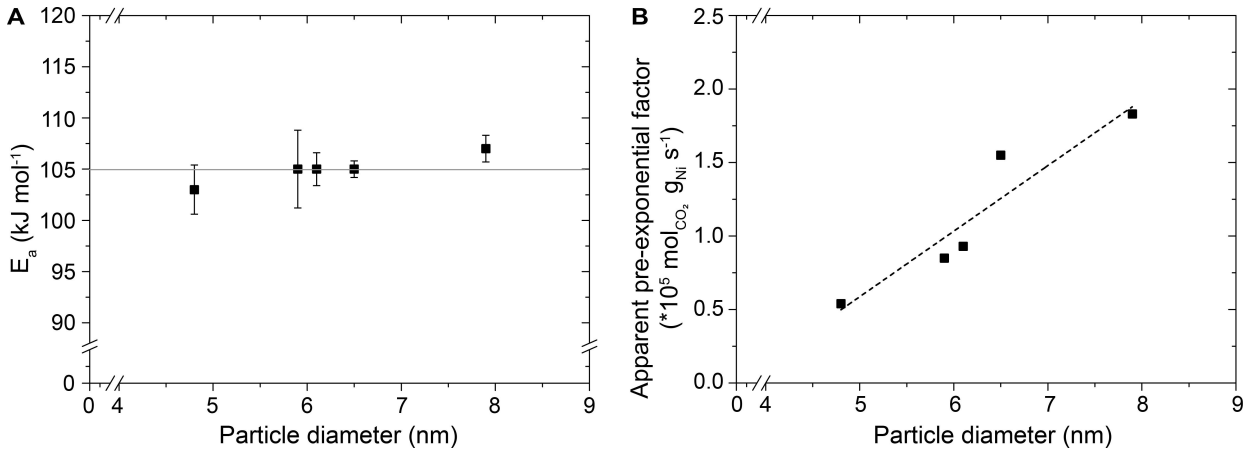

Figure 6. A) Apparent activation energy (E_a) in kJ mol^{-1} and **B**) the apparent pre-exponential factor calculated from the intercept of the Arrhenius plot (Figure S15) versus the particle diameter. Reaction conditions: CO_2 methanation at 240–300 °C and 30 bar, GHSV = 3500–5000 mL g_{cat}^{-1} h^{-1}.

particle size is likely related to the abundance in terrace sites, as also concluded for Ni/Al_2O_3 catalysts.[44]

The trend of increasing activity with increasing particle size differs from some previously reported studies on nickel based catalysts for CO_2 methanation. A particle size independence of the TOF was reported with the use of carbon nanotubes (3 to 9 nm)[33] as support. For Ni/SiO_2 catalysts (1–7 nm) tested at 1 and 20 bar, an optimum was found between 2–3 nm. The Ni loading was varied between 1 and 60 wt%,[14] which is a significantly larger range than used in this study. For Ni/CeO_2, mixed results were reported with either an increase in activity with increasing particle sizes from 3 to 46 nm,[34] or a decrease in activity with increasing particle sizes from 8 to 21 nm.[50] However, ceria can play a significant role itself activating CO_2, which could partly interfere with the particle size effect. Despite having studied a smaller Ni size range, we do not expect that for carbon supported nickel catalysts the TOF still increases significantly for Ni particles up to 50 nm, as the relative fraction in terrace sites does not change much anymore above 10 nm. This was also shown for Ni/Al_2O_3 (5–91 nm), where a particle size independence was reported for larger particles, despite high Ni loadings.[44] Overall, the differences observed could be due to several reasons including: i) the type of support used, ii) significant differences in Ni weight loading or iii) different reaction conditions applied. The latter can relate to, for instance, different H_2:CO_2 ratios (a 1:1 ratio is sometimes used to shift the focus towards the RWGS reaction[15]), gas hourly space velocities, reactor types, temperatures and pressures.

It would be very desirable to pinpoint directly which steps in the reaction mechanism are rate limiting and affected by the relative abundance of the different Ni facets with particle size, to fully unravel the observed particle size effect. However, it is important to consider that CH_4 formation and the RWGS reaction occur simultaneously, and the reaction rate is determined by a complex interplay between the concentrations of the different species present on the Ni surface. The partial pressures of H_2 and CO_2 were varied to determine the respective reaction orders for the 3.7_Ni/OxC, 4.1_Ni/OxC and 7.6_Ni/OxC catalysts. For all catalysts the initial conversion was kept around 15%. The moles of CO_2 converted hardly changed when varying the H_2 partial pressure, whereas a larger dependence on the CO_2 partial pressure was measured (shown for 7.6_Ni/OxC in Figure S16). For all Ni/OxC catalysts the reaction order with respect to H_2 was close to 0 (Table S6), indicating that the surface coverage and thus probably also the dissociation of H_2 was not limiting in this reaction. Although the reaction orders with respect to CO_2 were slightly higher (0.2–0.27) (Figure S17), they were far from first order kinetics. Hence the surface coverage of CO_2 did not seem to be highly limiting either. Besides, there was no clear dependence of the reaction order on the particle size. Reaction orders are highly temperature and pressure dependent.[5,40,51] Typical reaction order experiments have so far been performed at lower pressures than we report, where it is stated that the reaction order in H_2 decreased with increasing total pressure,[40,51] and the reaction order dependency in CO_2 was close to zero-order.[51] Thus, despite the different reaction conditions, our results match quite well with reported trends.

It was found that the binding strength of CO and the formation of different types of intermediates is particle size dependent and could steer the catalyst activity.[14] Especially sites such as steps, edges, kinks and corners play an important role in dissociating CO.[26,29–31] Both for direct and hydrogen assisted CO dissociation, the most favourable sites are step sites.[29,30] At the same time, low coordinated sites are also more prone to oxidation.[52] In Figure 2 we already displayed that the reducibility of Ni/OxC is particle size dependent and that the temperature of the passivated catalysts shifted to higher temperatures for the smaller nanoparticles. Subtle changes in oxidation state of nickel surface occur within a few minutes upon introduction or removal of CO_2 and/or H_2, revealing that nickel is very sensitive to the local atmosphere.[14,52] Mutz *et al.* showed that even after re-introducing H_2, the nickel surface might not get fully reduced anymore.[52] Besides oxidation by CO_2, also the formation of water should be taken into account. This might affect the oxidation of Ni nanoparticles, similar to

Fisher-Tropsch synthesis, where the oxidation of small cobalt crystallites is feasible.[53] For small particles, the contribution of the surface energy becomes important. The surface energy is higher for metallic nickel than for nickel oxide, comparing the values of the most stable surfaces (Ni(111) and NiO(100), Supporting Information section G). The chemical potential of Ni and NiO was calculated as function of particle size and H_2O/H_2 ratio. Depending on the H_2O/H_2 ratio used, a crossover from Ni to NiO was found for particle sizes below 2–5 nm, which indicates that smaller nickel particles could be oxidized (see Supporting Information section G, Figure S18 and S19). Given the errors in the calculation and assumptions, it cannot be excluded that for the catalysts with smaller nanoparticles, a significant fraction might be oxidized during catalysis, possibly decreasing the activity.

Finally, dynamics and possible changes in particle shape during catalysis could affect the activity. As recently shown by Frey *et al.*, metal nanoparticles can display fast dynamic changes under reaction conditions.[54] However, in this study long term analysis was performed to ensure measuring under steady state conditions. Possible local changes in shape, the number of different sites and defects present are probably averaged out over the time frame of our measurements.

Altogether our results show that up to 8 nm, larger particles positively steer the CO_2 hydrogenation activity, either directly due to enhanced activity of terrace sites or due to suppressed oxidation of the Ni surface.

Influence of particle size and pressure on selectivity

Apart from stability and activity, a third important factor that determines catalytic performance is selectivity. Figure 7A shows the CH_4 selectivity versus the CO_2 conversion for the catalysts with the smallest and largest nanoparticles at two different pressures. Overall, the CH_4 selectivity increased with increasing CO_2 conversion. Below 20% conversion, substantial amounts of CO were formed (Figure 7B). The conversion-dependence of the CH_4 selectivity suggests that the formation of CH_4 might occur via the intermediate formation of CO. The increase in CH_4 selectivity with increasing pressure (from 1 to 30 bar) is in line with earlier experimental results[55,56] and theory.[6] When the overall methanation reaction indeed proceeds via the RWGS reaction, the total reaction can be split up in two equations [Eqs. (2) and (3)]:

$$CO_2 + H_2 \leftrightarrows CO + H_2O \quad (\Delta H^0 = 41\ kJ\,mol^{-1},\ \Delta S^0 = 42.1\ J\,mol^{-1}\,K^{-1}) \tag{2}$$

$$CO + 3\,H_2 \leftrightarrows CH_4 + H_2O \quad (\Delta H^0 = -206\ kJ\,mol^{-1},\ \Delta S^0 = -214.64\ J\ mol^{-1}\,K^{-1}) \tag{3}$$

At high temperatures (>500 °C) and low pressures, the RWGS reaction is favoured, as it is an endothermic reaction. At low temperatures and high pressures, CO methanation is favoured, as it is an exothermic reaction. The temperature range used in this study thermodynamically favours the selectivity to CH_4, which can reach nearly 100% at both 1 and 30 bar (calculated with HSC Chemistry). The change in entropy is negative for methanation (equation 3), which is thus favoured at higher pressure, unlike the RWGS reaction. Thus, besides the positive effect on activity and a decreased chance for carbon deposition,[6,55] elevated pressures can help directing the selectivity to CH_4 instead of CO.

Apart from the influence of pressure, especially at low conversions the particle size is clearly influencing the selectivity to CH_4, as can be observed in Figure 7. The selectivity to CH_4 was highest for the largest nanoparticles, whereas the smallest nanoparticles produced relatively more CO. This trend confirmed the difference in selectivity already shown in Figure 3B. The full range of catalysts is shown in Figures S20–S22, where three ranges of particles sizes were identified: The CH_4 selectivity increased when going from 4–5 nm particles to 5.5–6.5 nm particles and finally to 7–8 nm particles. Similar

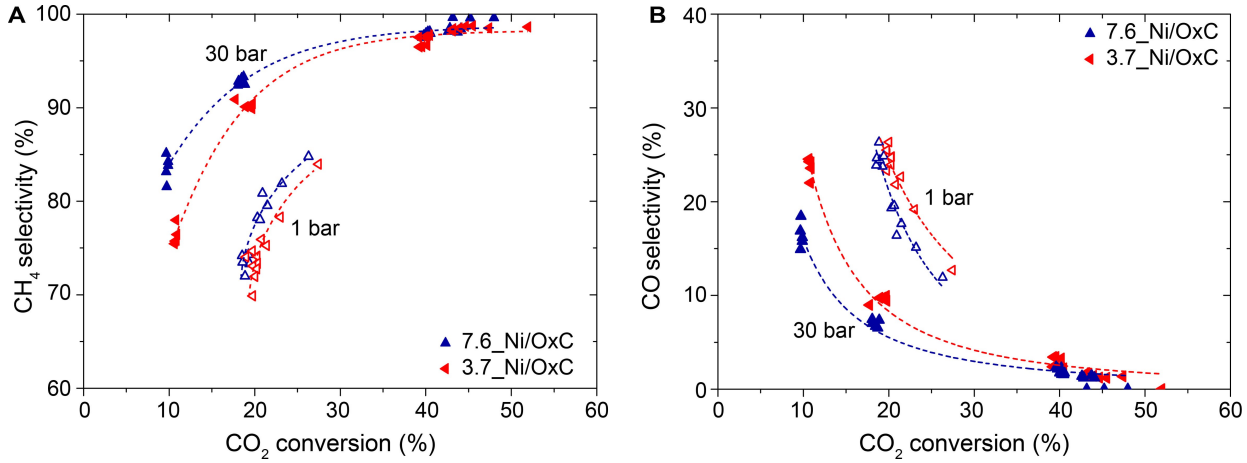

Figure 7. Influence of CO_2 conversion on product selectivity during CO_2 methanation at 1 and 30 bar pressure. **A**) CH_4 selectivity and **B**) CO selectivity vs CO_2 conversion at 1 bar (open symbols) and 30 bar (closed symbols). The dashed lines are used as guide for the eye. Reaction conditions: 300 °C, GHSV varied between 1000–2000 mL $g_{cat}^{-1}\,h^{-1}$ and 10000–23000 mL $g_{cat}^{-1}\,h^{-1}$.

effects have been reported at atmospheric pressure.[15,36,57] At 30 bar pressure, Millet *et al.* observed 100% selectivity to CO using single atom Ni/MgO catalysts, whereas the formation of CH_4 increased when particles up to 10 nm formed. They tested their catalysts at a CO_2 conversion <3 % and still observed significant CO formation,[35] which is in line with our results at low conversions. Wu *et al.* explained this particle size effect on CH_4 selectivity by a lower H_2 surface coverage of (sub-)nm particles compared to 9 nm particles at atmospheric pressure,[15] although this was questioned by Arpini *et al.*[58] From our reaction order study it is clear that the surface coverage of H_2 is not a relevant factor under our conditions (Table S6), as described before. Thus we were able to confirm that the selectivity trends are not related to the presence or absence of dissociated hydrogen on the Ni surface. The binding strength of CO could also be a factor to push the selectivity to CH_4 or CO.[59] Carbon coated Ni particles[58] or the formation of Ni_3C[59] species can affect the binding strength of CO and thus influence the selectivity. However, a Ni_3C phase was not observed in XRD before or after catalysis. Its formation was likely minimal, since Ni_3C should have compressed the selectivity to CH_4 almost completely at 1 bar.[59] This is not what we observed (Figure 7A). Overall, the present Ni/OxC catalysts exhibited the highest CO yield for the smallest nanoparticles (Figure S22), whereas high pressure CO_2 methanation and larger Ni particles (~8 nm) positively steered the CH_4 selectivity and methane yield.

Conclusions

We investigated the influence of particle size of Ni/OxC catalysts on the CO_2 methanation performance, with average particle diameters ranging from 3.7 to 7.6 nm (fresh catalysts). A sheetlike graphitic carbon support was used, functionalized with oxidic groups in order to reach reasonably stable catalysts. A 2 to 3-fold increase in activity (TOF) was observed with increasing particle diameters from 4.8 to 7.7 nm (after catalysis). While a similar activation energy for CO_2 conversion (~105 kJ mol^{-1} for all sizes) was observed, a 3-fold increase in apparent pre-exponential factor indicated that the intrinsic activity is likely related to the distribution of different surface sites. This could be either due to a higher activity of terrace sites or due to possibly reduced oxidation of the larger Ni particles. Similar activity trends were observed at high (30 bar) and low (1 bar) pressures. The highest CH_4 selectivity was obtained at high CO_2 conversions and high pressures, with 7.7 nm particles clearly having a higher intrinsic CH_4 selectivity than smaller particles. Overall, the use of larger Ni particles (~8 nm) is beneficial for both CO_2 conversion and the selectivity to CH_4 and is thus recommended for future catalyst design. It would be worthwhile to study the controlled synthesis of Ni/OxC catalysts with even larger Ni particles, to find an optimal performance.

Experimental Section

Catalyst synthesis

Nickel nitrate hexahydrate ($Ni(NO_3)_2 \cdot 6H_2O$, Sigma Aldrich, $\geq$97.0%), and nitric acid (HNO_3, Merck, 65%) were used as received. Silicon carbide (SiC, Alfa Aesar, $\geq$98.8%, 46 grit) was pressed and sieved in a 212–425 μm fraction, calcined at 800 °C for 10 h, washed with 65% HNO_3, subsequently rinsed with water until pH 7 was reached and finally dried at 120 °C overnight before use. Graphene nanoplatelets (GNP-500, ~500 m^2/g surface area, 0.9 mL g^{-1} pore volume, XG Sciences) were used as carbon support and oxidized to enhance wetting and to create anchoring points for the metal nanoparticles.[60] The functionalization was performed as reported in literature.[61] Approximately 10 g of the pristine GNP-500 was heated in 400 mL 65% HNO_3 to 80 °C for 2 h while stirring. Afterwards, the suspension was washed several times with 5 L demiwater each time until a pH of 6 was reached. After the last washing step, the support was dried at 120 °C for at least 24 h and subsequently crushed. This functionalized support is further referred to as OxC. After this treatment, the surface area was 380 m^2 g^{-1} and the total pore volume 0.68 mL g^{-1} (determined with N_2 physisorption at −196 °C on a Micromeritics TriStar II Plus apparatus). The amount of acidic surface groups had increased from 0.12 to 0.85 groups nm^{-1}, which was determined by base titration with NaOH using a TIM 880 titration setup by TitraLab.

A series of catalysts with various nickel particle sizes on the OxC support was prepared using incipient wetness impregnation. The concentration of the $Ni(NO_3)_2$ solution (and hence the nickel weight loading), decomposition temperature and/or reduction temperature were varied to obtain the series of catalysts. Typically, 1.5 g of oxidized carbon support was dried in a round-bottom flask for 90 min at 170 °C, while stirring under dynamic vacuum to remove water and air from the pores. Aqueous nickel nitrate solutions were prepared by dissolving $Ni(NO_3)_2$ with concentrations varying from 1 to 4 M in miliQ water. The solution was acidified with 0.10 M HNO_3 to ensure a pH around 1. The dried carbon support was impregnated to incipient wetness under static vacuum while stirring, to ensure that the solution was homogeneously spread over the support. The volume of the impregnation solution was 90% of the support pore volume, in order to avoid over-impregnation. Subsequently the sample was dried overnight at room temperature under dynamic vacuum before it was transferred to an argon glovebox.

To decompose the precursor, 1 gram of the sample was transferred to a plug-flow reactor and subjected to a heat treatment. The smallest Ni particles were obtained by decomposing the $Ni(NO_3)_2$ on carbon under 5% H_2/N_2 atmosphere during a direct reduction (2 °C min^{-1} to 300–400 °C for 180 min). Larger Ni particles were obtained by decomposing the nitrate in N_2 atmosphere (2 °C min^{-1} 300–400 °C for 90 minutes under 200 mL min^{-1} N_2). At least 300 °C was needed to completely decompose the nitrate and form NiO, which was confirmed with TGA-MS, a temperature similar to that found earlier for Ni/SiO_2.[62] This was followed by a reduction step at 300–400 °C (2 °C min^{-1}) for 90 minutes under 200 mL/min 5% H_2/N_2 flow to obtain metallic nickel particles. The largest particles were obtained by a heat treatment of the $Ni(NO_3)_2$ precursor $\geq$400 °C in N_2 atmosphere. In this case the support acted as reducing agent for NiO.[63] Finally the catalyst was slowly exposed to air to passivate the nickel particles. The exact parameters of the preparation of each catalyst are summarized in Table S1. The catalysts are denoted as *X*_Ni/OxC, where *X* is the surface averaged particle size of the fresh catalyst, determined with TEM.

Structural characterization

The catalysts were imaged with Transmission electron microscopy (TEM) on a FEI Talos L120 C operated at 120 kV. The catalyst sample was dispersed as a dry catalyst powder onto a Cu sample grid coated with holey carbon (Agar 300 mesh Cu). At least 400 nickel nanoparticles were manually counted per catalyst sample on at least 8 different catalyst locations. The number averaged particle diameter (d_n) and surface averaged particle dimeter (d_s) of nickel particles including their standard deviations were calculated using Equations (4) and (5):

$$d_n \pm \sigma_{dn} = \frac{1}{N} \sum_{i=1}^{N} d_i \pm \sqrt{\frac{1}{N} \sum_{i=1}^{N} (d_i - d_n)^2} \quad (4)$$

$$d_s \pm \sigma_{ds} = \frac{\sum_{i=1}^{N} d_i^3}{\sum_{i=1}^{N} d_i^2} \pm \sqrt{\frac{1}{N} \sum_{i=1}^{N} (d_i - d_s)^2} \quad (5)$$

where N indicates the total number of measured particles and d_i stands for the ith particle.

Powder X-ray diffraction (XRD) was performed on either a Bruker D2 or Bruker D8 powder X-ray diffractometer, equipped with a Co-$K_{a1,2}$ radiation source ($\lambda = 1.790$ Å) and a Lynxeye detector. This equipment was used to analyse as prepared and freshly reduced catalysts without exposure to air. After the reduction step, the catalyst was loaded into an airtight XRD specimen holder inside an Ar filled glovebox. To compare the catalysts before and after catalysis, both were slowly exposed to air at room temperature for passivation and subsequently measured on the Bruker D2. All samples were measured with diffraction angles varying between 10 and 95° 2θ with a step size of 0.05° 2θ/step. All diffractograms were normalized to the carbon (002) peak at 30.9°. The crystallite sizes were calculated by applying the Scherrer equation to the Ni^0 (111) peak at 50° after subtracting the diffractogram of oxidized carbon.

Thermogravimetric analysis was performed on a Perkin Elmer TGA800 coupled to an Hiden Analytical HPR-20 mass spectrometry (MS) system. This technique was used to determine the Ni weight loading of the catalysts before and after catalysis. 5–10 mg of the sample was first dried in Ar flow (100 mL min^{-1}) for 30 min at 120 °C. The sample was cooled down to 30 °C and the atmosphere was switched to 20% O_2/Ar flow (100 mL min^{-1}). Subsequently the sample was heated to 800 °C with a ramp of 10 °C min^{-1}, followed by a hold time of 10 min. Finally the sample was cooled down again to 30 °C to compare the mass before and after the heating ramp at the same temperature. The weight loading was calculated using Equation (6):

$$wt_{Ni} = \left(m_{rel,cat} - m_{rel,oxC}\right) \frac{M_{Ni}}{M_{NiO}} \quad (6)$$

Where $m_{rel,cat}$ and $m_{rel,OxC}$ are the relative mass (%) of the catalyst sample and bare oxidized support respectively after the measurement and M is the molar mass (g mol^{-1}). All nickel was assumed to be completely oxidized to NiO.

Temperature-programmed reduction (TPR) by H_2 was performed on a Micromeritics AutoChem II 2920 apparatus. Prior to the measurement, 40 mg catalyst (sieve fraction 75–150 μm) was dried at 120 °C under an Ar flow of 50 mL min^{-1} for 15 min. The sample was cooled down to room temperature, followed by a heating step in 5% H_2/Ar flow of 25 mL min^{-1} with 5 °C min^{-1} up to 800 °C. Reduction profiles were recorded with a thermal conductivity detector (TCD) and the outgoing gas was analysed using an mass spectrometer (MS) of Hiden Analytical equipped with a QGA Professional software package. H_2O was captured with a dry ice/isopropanol cold trap.

Temperature-programmed desorption (H_2-TPD) was performed on the same apparatus. 100 mg of catalyst was reduced at 300 °C in 5% H_2/Ar for 3 h and then cooled down to 5 °C. The gas was switched to 100% H_2 (15 mL min^{-1}) for 1 h. Then the gas was switched to Ar (15 mL min^{-1}) and the sample was flushed for 90 min before heating in Ar with 5 °C min^{-1} while recording the TCD signal and the H_2 MS signal.

H_2 chemisorption was measured on a Micromeritics ASAP 2020 C apparatus using ~100 mg of sample. Prior to the measurement, the sample was reduced in pure H_2 at 300 °C for 2 h (5 °C min^{-1}). The sample was then evacuated and cooled to 150 °C, and H_2 chemisorption was measured at that temperature.[64] Calculations to determine the dispersion and particle size from these measurements are reported in Supporting Information, section A.

Catalytic performance testing

The CO_2 methanation catalysis was performed in a high throughput gas-phase 16-parallel fixed bed reactor system (Avantium Flowrence). Prior to the catalytic test, the catalyst powders were pelletized using a hydraulic press and subsequently sieved into a fraction of 75–150 μm. The weight of nickel loaded in the reactor was kept constant at 4 mg, which was done by varying the total weight of catalyst loaded, based on the theoretical Ni loading of the catalysts after preparation. The catalysts were diluted approximately two times (based on weight) with SiC (212–425 μm) to prevent the formation of hotspots. The mixture of catalyst granules and SiC were loaded in stainless steel reactor tubes (2.6 mm inner diameter) on top of ~0.5 cm SiC granules. On top of the catalyst bed a layer of SiC was placed.

The Ni/OxC catalysts were *in situ* reduced prior to the reaction in a flow of 10% H_2/N_2 at 250 °C (2 °C min^{-1}) for 2.5 hours. Subsequently the reactors were cooled down to 120 °C before the reaction mixture was added. The reaction mixture consisted of CO_2:H_2:He = 19:76:5, 50 mL min^{-1}, and was divided over 16 reactors. Because the catalysts were tested in parallel with constant flow, the use of different total weights of catalyst resulted in using different GHSVs, of which the exact values are always indicated in the figure captions. The reactor was gradually pressurized to 30 bar and subsequently heated to the desired temperature with 2 °C min^{-1}. The catalytic tests were performed at temperatures ranging between 240 and 340 °C. Between isothermal stages, the temperature was increased or decreased with 2 °C min^{-1}. To vary the GHSV during a catalytic test the total flow over the 16 reactors was adapted while keeping the gas mixture the same. To study the influence of pressure, the pressure was varied between 1 and 30 bars several times within a single testing campaign. For the catalytic data shown in the result section, the exact details of the catalytic tests are described in the Supporting Information section I. The products were analysed directly with online gas chromatography (GC, Agilent 7890B) with a sampling time of 14 minutes. Thus when all 16 reactors were in use, each sample was analysed every ~4 h. The calculations of activity, turnover frequency (TOF), Arrhenius analysis and selectivity are explained in detail in the Supporting Information section I. After the reaction, the catalysts were flushed with He and left to cool down to 60 °C before exposing them to air. This resulted in controlled passivation for post-catalytic characterization.

Author contributions

N. V. and P. d. J. conceptualized the experiments. N. V. synthesized and characterized the catalysts with help from O. D., measured the performance of the catalysts, analysed the experimental data and wrote the manuscript. L. S. performed the H_2 chemisorption measurements. P. P. and F. S. performed the surface study calculations. J. W. d. R. provided technical support for the catalytic setup. All authors contributed to discussions of the results. J. v. d. H., O. D. and P. d. J. reviewed and edited the manuscript. All authors contributed to and agreed with the final manuscript.

Acknowledgements

The authors would like to thank Laura Barberis, Remco Dalebout and Giorgio Totarella for their support in the catalytic experiments. Dennie Wezendonk is kindly acknowledged for performing the TGA-MS experiments. This project is part of the Consortium on Metal Nanocatalysis funded by TotalEnergies OneTech Belgium, with reference TRTF Contract Ref IPA-5443.

Conflict of Interest

The authors declare no conflict of interest.

Data Availability Statement

The data that support the findings of this study are available from the corresponding author upon reasonable request.

Keywords: Carbon Dioxide · Nickel · Methanation · Particle size · Pressure

[1] M. Specht, J. Brellochs, V. Frick, B. Sturmer, U. Zuberbuhler, M. Sterner, R. Waldstein, *Erdöl Erdgas Kohle* **2010**, *126*, 342–346.
[2] G. Centi, E. A. Quadrelli, S. Perathoner, *Energy Environ. Sci.* **2013**, *6*, 1711–1731.
[3] P. A. U. Aldana, F. Ocampo, K. Kobl, B. Louis, F. Thibault-Starzyk, M. Daturi, P. Bazin, S. Thomas, A. C. Roger, *Catal. Today* **2013**, *215*, 201–207.
[4] P. Sabatier, J. B. Senderens, *CR Acad. Sci. Paris* **1902**, *134*, 514–516.
[5] T. Burger, P. Donaubauer, O. Hinrichsen, *Appl. Catal. B* **2021**, *282*, 1–22.
[6] J. Gao, Y. Wang, Y. Ping, D. Hu, G. Xu, F. Gu, F. Su, *RSC Adv.* **2012**, *2*, 2358–2368.
[7] http://www.hsc-chemistry.net/, **2022**.
[8] J. Kopyscinski, T. J. Schildhauer, S. M. A. Biollaz, *Fuel* **2010**, *89*, 1763–1783.
[9] S. Rönsch, J. Schneider, S. Matthischke, M. Schlüter, M. Götz, J. Lefebvre, P. Prabhakaran, S. Bajohr, *Fuel* **2016**, *166*, 276–296.
[10] B. Alrafei, I. Polaert, A. Ledoux, F. Azzolina-Jury, *Catal. Today* **2020**, *346*, 23–33.
[11] M. Thema, F. Bauer, M. Sterner, *Renewable Sustainable Energy Rev.* **2019**, *112*, 775–787.
[12] M. Gruber, P. Weinbrecht, L. Biffar, S. Harth, D. Trimis, J. Brabandt, O. Posdziech, R. Blumentritt, *Fuel Process. Technol.* **2018**, *181*, 61–74.
[13] R. Chauvy, N. Meunier, D. Thomas, G. De Weireld, *Appl. Energy* **2019**, *236*, 662–680.
[14] C. Vogt, E. Groeneveld, G. Kamsma, M. Nachtegaal, L. Lu, C. J. Kiely, P. H. Berben, F. Meirer, B. M. Weckhuysen, *Nat. Catal.* **2018**, *1*, 127–134.
[15] H. C. Wu, Y. C. Chang, J. H. Wu, J. H. Lin, I. K. Lin, C. S. Chen, *Catal. Sci. Technol.* **2015**, *5*, 4154–4163.
[16] B. Miao, S. S. K. Ma, X. Wang, H. Su, S. H. Chan, *Catal. Sci. Technol.* **2016**, *6*, 4048–4058.
[17] J. H. Kwak, L. Kovarik, J. Szanyi, *ACS Catal.* **2013**, *3*, 2094–2100.
[18] S. Kattel, B. Yan, J. G. Chen, P. Liu, *J. Catal.* **2016**, *343*, 115–126.
[19] R. A. Van Santen, *Acc. Chem. Res.* **2009**, *42*, 57–66.
[20] M. Schumann, M. R. Nielsen, T. E. L. Smitshuysen, T. W. Hansen, C. D. Damsgaard, A.-C. A. Yang, M. Cargnello, J.-D. Grunwaldt, A. D. Jensen, J. M. Christensen, *ACS Catal.* **2021**, *11*, 5189–5201.
[21] E. Vesselli, M. Rizzi, L. de Rogatis, X. Ding, A. Baraldi, G. Comelli, L. Savio, L. Vattuone, M. Rocca, P. Fornasiero, A. Baldereschi, M. Peressi, *J. Phys. Chem. Lett.* **2010**, *1*, 402–406.
[22] C. Mebrathu, F. Krebs, S. Abate, S. Perathoner, G. Centi, R. Palkovits, *Stud. Surf. Sci. Catal.* **2019**, *178*, 85–103.
[23] K. Jalama, *Catal. Rev.* **2017**, *59*, 95–164.
[24] T. Noor, Y. Qi, D. Chen, *Appl. Catal. B* **2020**, *264*, 118430.
[25] C. H. Bartholomew, R. B. Pannell, J. L. Butler, *J. Catal.* **1980**, *65*, 335–347.
[26] Z. P. Liu, P. Hu, *J. Am. Chem. Soc.* **2003**, *125*, 1958–1967.
[27] J. Gao, C. Jia, M. Zhang, F. Gu, G. Xu, F. Su, *Catal. Sci. Technol.* **2013**, *3*, 2009–2015.
[28] D. Beierlein, D. Häussermann, M. Pfeifer, T. Schwarz, K. Stöwe, Y. Traa, E. Klemm, *Appl. Catal. B* **2019**, *247*, 200–219.
[29] M. P. Andersson, F. Abild-Pedersen, I. N. Remediakis, T. Bligaard, G. Jones, J. Engbæk, O. Lytken, S. Horch, J. H. Nielsen, J. Sehested, J. R. Rostrup-Nielsen, J. K. Nørskov, I. Chorkendorff, *J. Catal.* **2008**, *255*, 6–19.
[30] J. Engbæk, O. Lytken, J. H. Nielsen, I. Chorkendorff, *Surf. Sci.* **2008**, *602*, 733–743.
[31] J. X. Liu, B. Y. Zhang, P. P. Chen, H. Y. Su, W. X. Li, *J. Phys. Chem. C* **2016**, *120*, 24895–24903.
[32] C. Vogt, M. Monai, E. B. Sterk, J. Palle, A. E. M. Melcherts, B. Zijlstra, E. Groeneveld, P. H. Berben, J. M. Boereboom, E. J. M. Hensen, F. Meirer, I. A. W. Filot, B. M. Weckhuysen, *Nat. Commun.* **2019**, *10*, 1–10.
[33] J. Gödde, M. Merko, W. Xia, M. Muhler, *J. Energy Chem.* **2021**, *54*, 323–331.
[34] E. Marconi, S. Tuti, I. Luisetto, *Catalysts* **2019**, *9*, 375.
[35] M. M. Millet, G. Algara-Siller, S. Wrabetz, A. Mazheika, F. Girgsdies, D. Teschner, F. Seitz, A. Tarasov, S. V. Levchenko, R. Schlögl, E. Frei, *J. Am. Chem. Soc.* **2019**, *141*, 2451–2561.
[36] J. H. Kwak, L. Kovarik, J. Szanyi, *ACS Catal.* **2013**, *3*, 2449–2455.
[37] A. Tuxen, S. Carenco, M. Chintapalli, C. H. Chuang, C. Escudero, E. Pach, P. Jiang, F. Borondics, B. Beberwyck, A. P. Alivisatos, G. Thornton, W. F. Pong, J. Guo, R. Perez, F. Besenbacher, M. Salmeron, *J. Am. Chem. Soc.* **2013**, *135*, 2273–2278.
[38] W. Wang, W. Chu, N. Wang, W. Yang, C. Jiang, *Int. J. Hydrogen Energy* **2016**, *41*, 967–975.
[39] H. Mansour, E. Iglesia, *J. Am. Chem. Soc.* **2021**, *143*, 11582–11594.
[40] R. Z. C. Meerten, J. G. Vollenbroek, M. H. J. M. de Croon, P. F. M. T. van Nisselrooy, J. W. E. Coenen, *Appl. Catal.* **1982**, *3*, 29–56.
[41] T. Herwijnen, H. Doesburg, W. A. de Jong, *J. Catal.* **1973**, *28*, 391–402.
[42] F. Rodríguez-Reinoso, A. Sepúlveda-Escribano, in *Carbon Materials for Catalysis.*, **2009**, pp. 131–155.
[43] C. Louis, Z. X. Cheng, M. Che, *J. Phys. Chem.* **1993**, *97*, 5703–5712.
[44] D. Beierlein, D. Häussermann, M. Pfeifer, T. Schwarz, K. Stöwe, Y. Traa, E. Klemm, *Appl. Catal. B* **2019**, *247*, 200–219.
[45] O. Daoura, G. Fornasieri, M. Boutros, N. El Hassan, P. Beaunier, C. Thomas, M. Selmane, A. Miche, C. Sassoye, O. Ersen, W. Baaziz, P. Massiani, A. Bleuzen, F. Launay, *Appl. Catal. B* **2021**, *280*, 119417.
[46] F. Yang, D. Liu, Y. Zhao, H. Wang, J. Han, Q. Ge, X. Zhu, *ACS Catal.* **2018**, *8*, 1672–1682.
[47] J. H. Bitter, M. K. Van Der Lee, A. G. T. Slotboom, A. J. Van Dillen, K. P. De Jong, *Catal. Lett.* **2003**, *89*, 139–142.
[48] M. Zieliński, R. Wojcieszak, S. Monteverdi, M. Mercy, M. M. Bettahar, *Int. J. Hydrogen Energy* **2007**, *32*, 1024–1032.
[49] R. van Hardeveld, F. Hartog, *Surf. Sci.* **1969**, *15*, 189–230.
[50] Z. Hao, J. Shen, S. Lin, X. Han, X. Chang, J. Liu, M. Li, X. Ma, *Appl. Catal. B* **2021**, *286*, 119922.
[51] G. D. Weatherbee, C. H. Bartholomew, *J. Catal.* **1982**, *77*, 460–472.
[52] B. Mutz, A. M. Gänzler, M. Nachtegaal, O. Müller, R. Frahm, W. Kleist, J. D. Grunwaldt, *Catalysts* **2017**, *7*, 279.
[53] E. Van Steen, M. Claeys, M. E. Dry, J. Van De Loosdrecht, E. L. Viljoen, J. L. Visagie, *J. Phys. Chem. B* **2005**, *109*, 3575–3577.

[54] H. Frey, A. Beck, X. Huang, J. A. van Bokhoven, M. G. Willinger, *Science* **2022**, *376*, 982–987.
[55] L. Jürgensen, E. A. Ehimen, J. Born, J. B. Holm-Nielsen, *Bioresour. Technol.* **2015**, *178*, 323–329.
[56] W. L. Vrijburg, G. Garbarino, W. Chen, A. Parastaev, A. Longo, E. A. Pidko, E. J. M. Hensen, *J. Catal.* **2020**, *382*, 358–371.
[57] K. Feng, J. Tian, M. Guo, Y. Wang, S. Wang, Z. Wu, J. Zhang, L. He, B. Yan, *Appl. Catal. B* **2021**, *292*, 120191.
[58] B. H. Arpini, A. H. Braga, L. R. Borges, P. Vidinha, R. V. Gonc, J. Szanyi, L. M. Rossi, *ACS Sustainable Chem. Eng.* **2022**, *10*, 2331–2342.
[59] T. S. Galhardo, A. H. Braga, B. H. Arpini, J. Szanyi, R. V. Gonçalves, B. F. Zornio, C. R. Miranda, L. M. Rossi, *J. Am. Chem. Soc.* **2021**, *143*, 4268–4280.
[60] J. L. Figueiredo, *J. Mater. Chem. A* **2013**, *1*, 9351–9364.
[61] B. Donoeva, N. Masoud, P. E. De Jongh, *ACS Catal.* **2017**, *7*, 4581–4591.
[62] J. R. A. Sietsma, H. Friedrich, A. Broersma, M. Versluijs-helder, A. J. van Dillen, P. E. de Jongh, K. P. de Jong, *J. Catal.* **2008**, *260*, 227–235.
[63] Y. Yang, L. Jia, B. Hou, D. Li, J. Wang, Y. Sun, *Catal. Sci. Technol.* **2014**, *4*, 717–728.
[64] C. Hernández Mejía, J. E. S. Van Der Hoeven, P. E. De Jongh, K. P. De Jong, *ACS Catal.* **2020**, *10*, 7343–7354.

Manuscript received: May 24, 2022
Revised manuscript received: August 29, 2022
Accepted manuscript online: September 23, 2022
Version of record online: October 25, 2022